communications biology

Article

https://doi.org/10.1038/s42003-024-06710-8

RRmorph—a new R package to map phenotypic evolutionary rates and patterns on 3D meshes

Check for updates

Marina Melchionna[1], Silvia Castiglione[1], Giorgia Girardi[1], Carmela Serio[1], Antonella Esposito[1], Alessandro Mondanaro[2], Antonio Profico[3], Gabriele Sansalone[4] & Pasquale Raia[1]

The study of evolutionary rates and patterns is the key to understand how natural selection shaped the current and past diversity of phenotypes. Phylogenetic comparative methods offer an array of solutions to undertake this challenging task, and help understanding phenotypic variation in full in most circumstances. However, complex, three-dimensional structures such as the skull and the brain serve disparate goals, and different portions of these phenotypes often fulfil different functions, making it hard to understand which parts truly were recruited by natural selection. In the recent past, we developed tools apt to chart evolutionary rate and patterns directly on three-dimensional shapes, according to their magnitude and direction. Here, we present further developments of these tools, which now allow to restitute the mapping of rates and patterns with full biological realism. The tools are condensed in a new R software package.

Changes in the rate of phenotypic evolution arise because of natural selection[1–3]. Consequently, comparative studies address rate variation to test specific evolutionary hypotheses such as adaptive radiation[4–6], stasis[7], reduction in the strength of selection towards specific phenotypes[8], or density-dependent trait evolution[9,10]. Currently available statistical tools compute rates in terms of the amount of trait variance added over the evolutionary time[11], for the phenotype as a whole (e.g. multivariate phenotypic disparity[12,13]), or for a scalar dimension (e.g. body size[14,15]). However, the rate of trait change may depend on—or affect only—a limited portion of the phenotype, as with the appearance of key innovations[16–18], selection for larger appendages or weapons[19,20], or for different limb lengths[21]. Still, functional diversity may be unrelated to the portion of the phenotype involved, as with morphologically diverse structures that perform similarly (many-to-one mapping[22–24]) making it crucial to understand rate variation of the structure of interest in the context of the whole phenotype[25]. Recently, we demonstrated our own phylogenetic comparative method, *RRphylo*[26] can be used to chart the phenotypic evolutionary rates magnitude of change across the phenotype[27,28]. This is because *RRphylo* rates are represented by phylogenetic ridge regression slopes describing the amount and direction of phenotypic change from one node to the next across the tree, fitted simultaneously for the entire tree by means of L2 regularization[26,29], which minimizes rate variation across the tree branches. As applied on Principal Component (PC) scores derived from the decomposition of shape variation for 3D data, the *RRphylo* rates describe changes in the PC scores, which in turn can be translated into deformations of a reference shape, thus allowing the PC rates to be charted across the 3D phenotype. In the original version, this rate mapping procedure was embedded in the 'RRphylo' package functions *rate.map* and *conv.map*, which by the same workflow can map either rates (the former) or areas of the phenotype responsible for morphological convergence (the latter[28]). One potential limitation of these algorithms is that since rates (or pattern of convergence) are mapped on the 3D shapes reconstructed by rotating and translating PC scores back into configuration space using selected PC axes only, they do not provide the morphological details detectable from the original 3D mesh. Hence, the portion of the phenotype affected by the most important shape changes must be understood by their gross anatomy. Here, we present an updated version of *rate.map* and *conv.map*, condensed in a new R package, 'RRmorph', which now allows transporting the rate variation directly on the real phenotype, allowing to inspect how rates unfold over the phenotype with the level of details provided with the original 3D meshes.

Here, we used the 'RRmorph' toolkit to study the evolution of brain shape in primates, and morphological convergence in primate brains and skulls. The rationale for the former study is to highlight which areas of the brain enlarged the most during the evolution of the group. Primates are known to perform particularly well in complex cognitive tasks including tactical deception and understanding the mental states of conspecifics[30,31]. These functions, which are acutely pronounced in catarrhines (and even more in apes) are usually connected to the evolutionary enlargement of the

[1]DiSTAR, University of Naples Federico II, Naples, Italy. [2]DST, University of Florence, Florence, Italy. [3]Department of Biology, University of Pisa, Pisa, Italy. [4]Department of Life Sciences, University of Modena and Reggio Emilia, Modena, Italy. e-mail: marina.melchionna@unina.it; pasquale.raia@unina.it

prefrontal cortex[32,33]. Yet, the issue of whether apes and humans really have expanded prefrontal areas is debated[34,35]. We predict that high rates of cortical expansion must accrue to the prefrontal area in primates starting from early forms towards the ape branch of the primate tree if prefrontal area enlargement was provided by natural selection.

The second case study addresses patterns of convergence in primate brains and skulls. Convergence between distant species' brains is expected to occur if selection favored the enlargement of specific cortical areas over other in response to species ecology and lifestyles[36]. Similarly, structures of the skull linked to vision acuity, like forward facing orbits and enlarged orbits in nocturnal euprimate species, can be either the result of morphological convergence or shared inheritance from stem primates[37,38]. We do expect convergence in clades exhibiting similar ecological requirements to be located in the brain and skull areas linked to the species ecology.

Results

Relative Warp Analysis (RWA)

We found that the distribution of endocast shapes on the Relative Warp 1 (RW1) to Relative Warp 2 plot (explaining 50.6% and 14.9% of the total variance, respectively) indicates a clear distinction between adapids, prosimians (Strepsirrhini plus tarsiers) and Catarrhini. Hominids detached from the other primates on the positive values of both axes. *Rooneyia viejaensis* is located next to the other prosimians (Fig. 1a). We developed a specific function named *plotland* (still embedded in 'RRmorph') to show the relative importance of landmarks and semilandmarks displacement on each PC or RW axis (PCA loadings). On the first RW axis (Fig. 1a) the major variation pertains to the dorso-parietal and cerebellum areas. Strepsirrhine and prosimians have flat endocasts, which is rounded in apes and monkeys. The shape variation on the temporo-parietal portion of the endocast discriminates Primate clades on RW2, with Omomyidae and Adapidae and hominids placing at opposite positions in the morphospace (i.e. the opposite ends of the RW axes).

The representation of the first two axes of the RWA on the skull dataset shows a marked separation between prosimians, monkeys plus apes, and humans (Fig. 1b). The hominids position in the morphospace is unique except for *Australopithecus africanus* standing close to *Pan troglodytes*. The areas which appear to be more important in the definition of the morphospace along RW1 are the nasal bones and the cranial vault (positive values) and the maxilla (negative values). On RW2 the greatest importance is linked to the shape of the orbits and the tooth row (Fig. 1b).

rate.map case study

We find the highest rates of endocast shape evolution accrue to the human clade (Fig. 2). To locate which areas evolved more rapidly through the evolutionary history of primates and how they changed, we charted the rates effect on seven different 3D mesh surfaces belonging to *Rooneyia viejaensis*, *Eulemur mongoz*, *Adapis parisiensis*, *Macaca mulatta*, *Homo sapiens*, *Alouatta guariba* and *Cebus albifrons* (Fig. 2). The Primate cranial capacity increased through the primate evolution, especially in Catharrini and Platyrrhini. Much of this expansion is related to the frontal and prefrontal areas, especially in Catharrhini. Among Platyrrhini, the endocast of *Alouatta* presents a small degree of enlargement in the same areas, being almost comparable with the prosimians. The occipital area enlargement, together with the expansion of the cerebellum, is particularly notable in the genus *Homo*. *Adapis*, a basal Primate from the Eocene, shows an opposite pattern, with relatively small frontal and occipital areas. *Rooneyia* differs from others Eocene primates, as only a slight enlargement of the frontal and temporal area is visible.

To visualize the cortical areas affected by high rate of evolution, we used a digital reproduction of MRI image of the same individual of *H. sapiens* showed in Fig. 2. We sampled 18 landmarks directly on the MRI brain surface. Then, we transferred the semilandmarks patch of the corresponding *H. sapiens* endocast specimen on the brain surface by using the thin plate spline algorithm (*tps3d* function in 'Morpho' R package). Eventually, we used Morpho's *slider3d* algorithm on both endocast and MRI semilandmarks sets to minimize the differences between them. The cortical expansion/contraction patterns on the MRI were eventually interpolated as for the endocasts by using the *interpolMesh* algorithm in 'RRmorph' (Fig. 3).

conv.map case study on skulls

search.conv revealed marginally significant convergence in skull shape among Lemuroidea (i.e. *Archaeolemur*, *Indri*, *Lemur*, *Eulemur*, *Hapalemur*, *Propithecus*) and the howler monkey *Alouatta* genus (mean angle = 0.662, *p*-value = 0.04). *conv.map* showed the convergent areas between Lemuroidea and *Alouatta* are mostly related to the splanchnocranium and the top of the skull, and to nasal, maxillary and frontal bones in particular (Fig. 4).

conv.map case study on endocast and skulls

The convergence investigation among the resized and comparable dataset of endocast and skulls revealed significant convergence among the same clades, which mean *Alouatta* and Lemuroidea (*search.conv* on skulls: mean angle = 0.662, *p*-value = 0.05; *search.conv* on endocasts: mean angle = 0.738, *p*-value = 0.04, Supplementary Figs. 1 and 2).

Discussion

Natural selection operates on phenotypes adapting their shape to the functions they perform. However, the evidence for adaptation is masked by the effects of phylogenetic inheritance, by convergence of function without convergence of shape[22,23], and by the limits imposed by genetic, developmental, and morphological constraints[39–42]. With complex, multipurpose structures such as the skull or the brain, disentangling the effects of selection and constraints is further complicated by the fact that different parts of the phenotype (i.e. the structure) may evolve under different selection regimes, and that selection on one portion of the phenotype may affect indirectly other portions to provide proper functioning and balance between different selection pressures[43]. For example, it is well understood that the now extinct sabertooth cats evolved long upper canines to deliver their bite[44–46]. Yet, also the increased gape, low position of the skull to mandible articulation, and protruding incisors, are all surmised to be part of this killing method toolkit, meaning that high rate of evolution should extend to these areas as well[28]. Patterns of selection can be inferred directly from phylogenetic and phenotypic data[3,26,47]. Yet, most phylogenetic comparative methods calculate rates as a scalar, representing some form of trait variance accumulated over time[48] or some standardized measure of trait change over time (e.g. *darwin*, *haldane*) which implies that although trait variation across the branches of the phylogeny and over time can be readily assessed, charting rate variation over the phenotype is impossible. Our *RRphylo* method derives the rates from the phylogeny and data, as represented by the L2 regression slope between the nodes in the tree. As applied to shape decomposition (PC axes) data, this means rates can be translated back into localized shape changes[27,28] allowing the rate variation to be visualized on the phenotype. In this study, we extended our original rate charting method to transfer the map of rates directly on the real phenotype. We applied the new techniques, condensed in a new R package named 'RRmorph', to the evolution of brain and skull shape in primates. We found that particularly high rates of cortical expansion accrue to the prefrontal area in catarrhine, and especially so in the human prefrontal cortex (Fig. 2). This finding agrees with several reports emphasizing prefrontal expansion in our species and fellow apes[32,33,49] and with the decisive role that this area of the cortex performs in producing exquisitely complex, higher-order cognitive functions including moral judgment, social agency and decision making[50–53]. However, the notion of greatly expanded prefrontal cortex in humans and apes (at least) was strongly criticized[34,35]. We found that rapid expansion of the prefrontal cortex characterized the evolution of primates, extending to species other than apes (Fig. 2). In humans, rapid expansion pertains to the posterior parietal cortex and the cerebellum as well (Fig. 3), pointing to the key role of these areas in higher-order cognition in our species[54,55]. As a second case study, we explored patterns of convergence in primate skulls. Although not particularly strong, we found intriguing evidence that howler monkey skulls

converge on lemurs' (Fig. 4). The peculiar skull shape of *Alouatta* has long been noted. Howler monkeys present a peculiar retroflexion of the facial skeleton on the cranial base (a condition known as airorynchy) and posteriorly oriented foramen magnum[56] which are not present in any other New World monkey, but only occurs in a few apes (*Pongo*[57]) and prosimians[58,59], respectively. Interestingly, the only species to present both conditions, to our knowledge, is the extinct lemur *Megaladapis*[60], which has been used as evidence that both genera converge on strictly folivorous

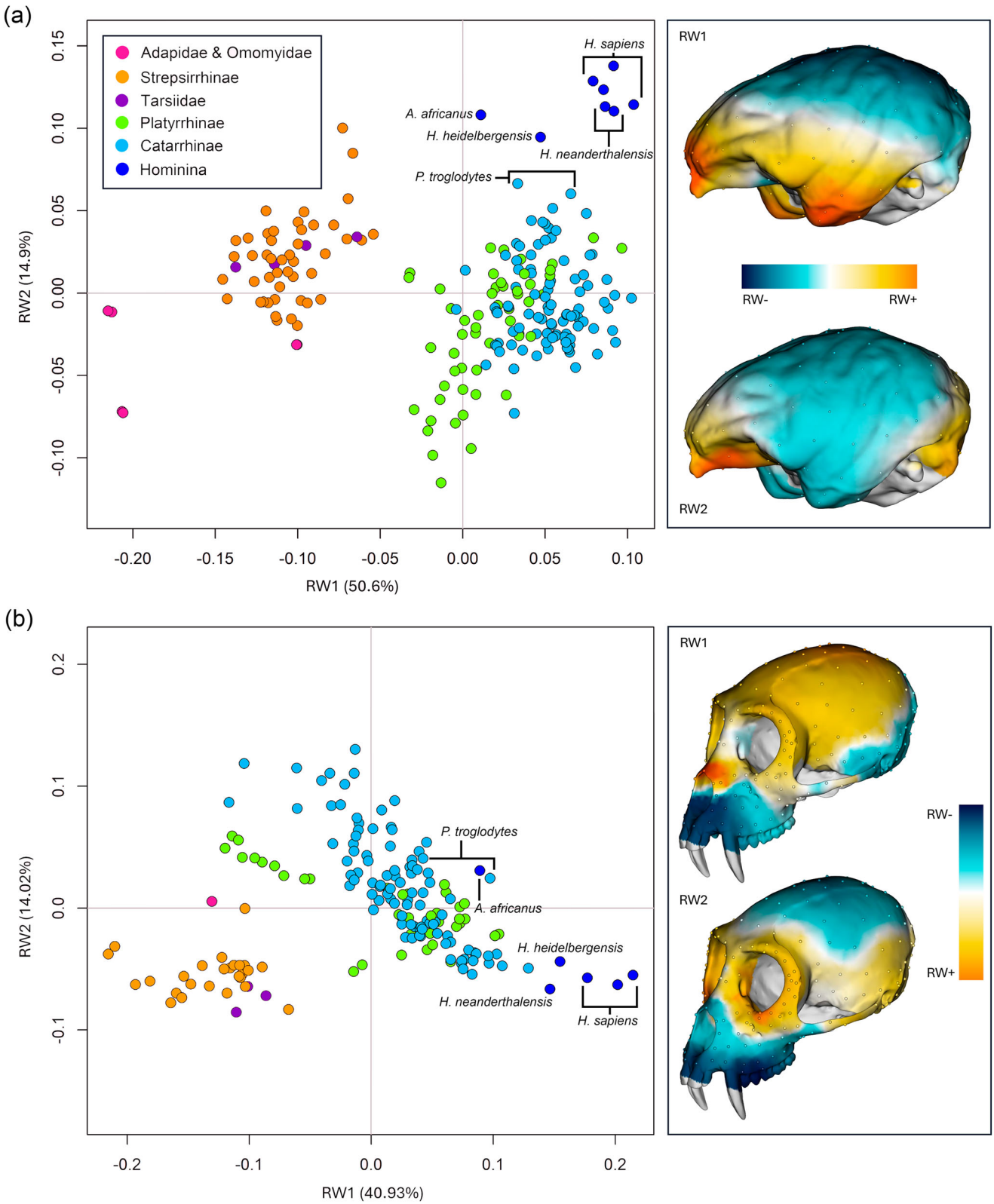

Fig. 1 | Morphospace analysis for endocast and skull datasets. a RW1 to RW2 plot on the endocast dataset. To the right, the output of 'RRmorph' *plotland* function. The endocast used for the image belongs to *Presbytis potenziani* USNM-121668. **b** Plot of the first two Relative Warp axes of the RWA on the skull dataset. On the right, the output of *plotland* function. The specimen used for the representation is *Cercopithecus ascanius* USNM-452510.

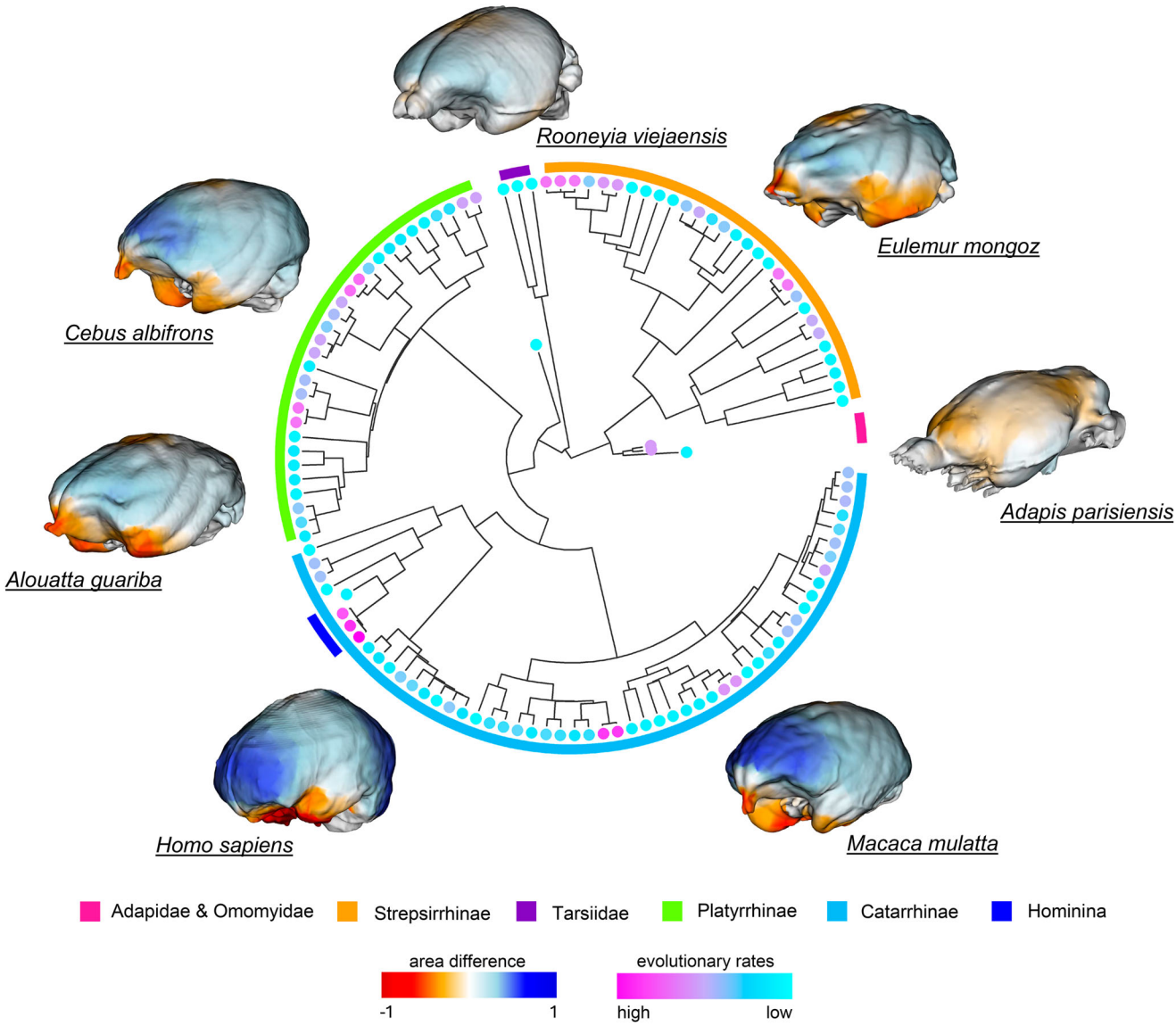

Fig. 2 | The Primate phylogenetic tree and representative endocasts of the major groups. Tips are colored based on the magnitude of multivariate rates of endocast shape evolution. The color gradient of the surfaces indicates the difference of each species from the shape at the tree root in terms of cortical expansion (blue) and contraction (red).

diet[60,61]. We repeated the same convergence test on both skull and brains, retrieved from the same specimens. The results confirmed convergence between lemurs and *Alouatta* for both structures. *conv.map* found convergence between the two clades regard the top of the skull, the nasal and maxillary bones, and the zygomatic arch (Supplementary Fig. 1), and the top of the brain around the fronto-pariental juncture (Supplementary Fig. 2), in keeping with the observation that *Alouatta* has vertically flattened and relatively small brains due to the early cessation of brain growth and early closure of the skull sutures[56]. It is hard to tell whether the patterns of convergence we found have strong functional significance. Tree foliage eating is not restricted to lemurs and howler monkey, and it is *Megaladapis*, rather than extant lemurs, to show airorynchy. Issues of convergence with no functional meaning are not rare[23,62]. In the case we dealt with, it is possible that developmental constraint acting on the braincase and skull and brain growth make howler monkey to resemble lemurs, rather than the two evolving towards a shared portion of the primate head morphospace.

This study highlights the potential utility of 'RRmorph' toolkit to study how evolutionary change unfolds upon phenotypic structures. By charting evolutionary rates and patterns directly on the phenotype, with unprecedented levels of details, these tools offer new and improved levels of investigation to understand the diversity of shape and its functional underpinning which we hope will stimulate future research on these fascinating issues.

Materials and methods

Data collection

We built two different databases for different phenotypes. The endocasts database includes 211 3D digital models representing 120 primate species. The skulls database comprises 179 3D digital models belonging to 93 different primate species. For both databases we included both a male and a female individual, where available. The digital models come from different institutions. Details about the collections are reported in Supplementary Data 1. On each digital model, 18 landmarks on endocasts and 41 landmarks on crania were manually sampled by using Amira software[63]. Collected landmarks were of type I (homologous structure) and II (geometric homologous structure, i.e. point of maximum curvature). The landmarks are described in Supplementary Tables 1 and 2, and shown in Figs. 5 and 6. Missing landmarks were estimated using the functions *fixLMmirror* and *fixLMtps* in 'Morpho' R package[64].

We performed a preliminary alignment of the landmark configurations, for both endocasts and crania, to identify the specimen closest to the consensus shape. Their respective 3D surfaces were chosen as reference. By

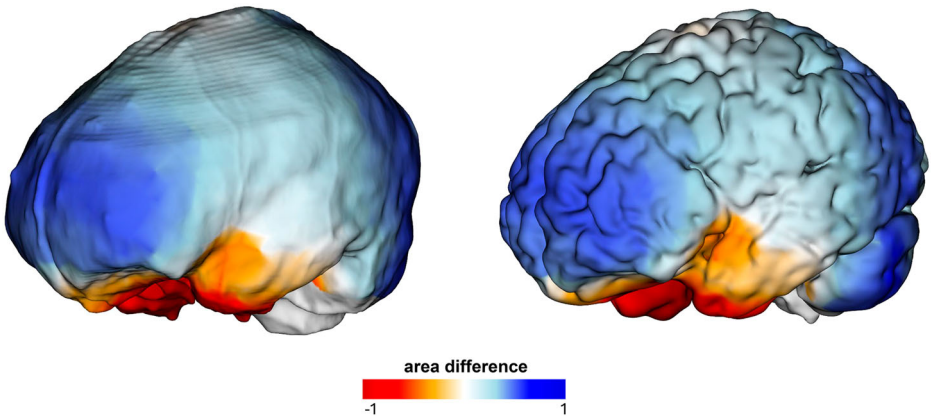

Fig. 3 | Patterns of evolutionary shape change in *Homo sapiens*. On the left, the shape change is mapped on the reconstructed endocast. On the right, the same variation is mapped on the brain cortex[75]. The shape change is described in terms of expansion (blue) and contraction (red) compared to the basal primate condition.

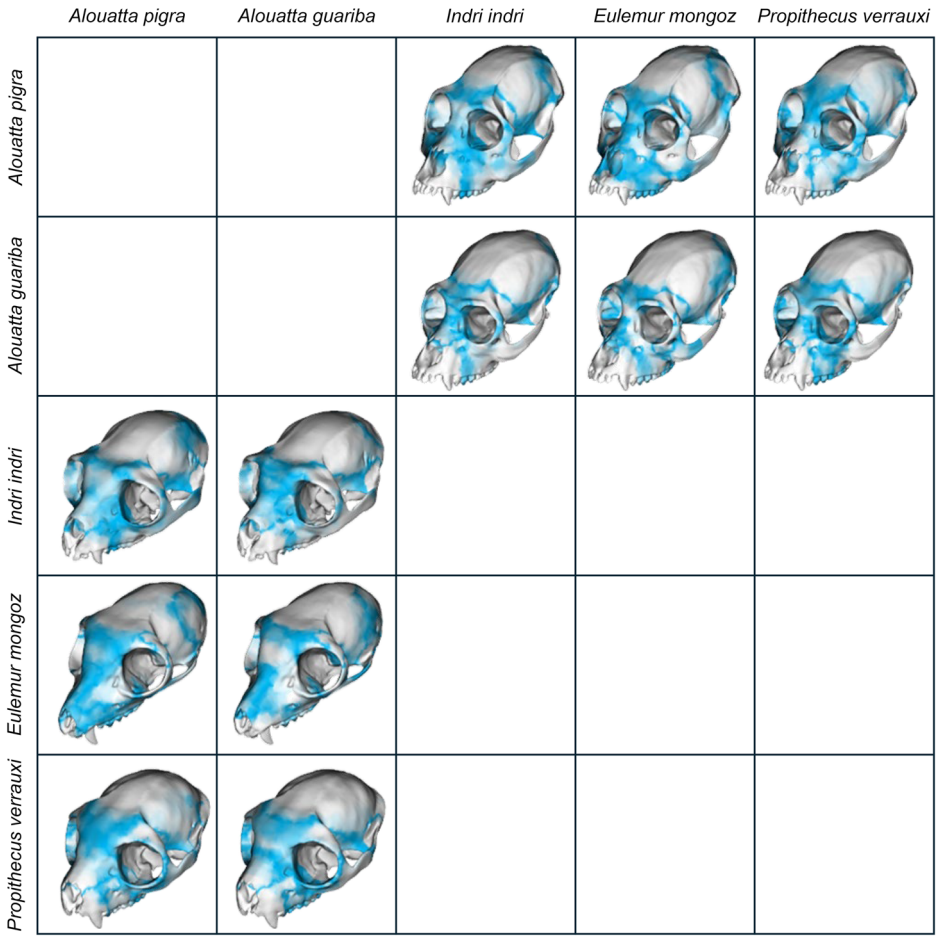

Fig. 4 | *conv.map* applied to the skulls of lemurs and howler monkey, found to converge morphologically on each other. The skull areas responsible for the convergence pattern are colored in blue shades. The grid reports pairwise convergence patterns depicted on the original phenotypes. For all pairwise comparisons, the same shape variables found to explain convergence (RW axes) were used.

applying this procedure, we selected *Presbytis potenziani* USNM-121668 for the endocast data and *Cercopithecus ascanius* USNM-452510 for the skulls. Semilandmarks were automatically sampled on the right side of both reference digital surfaces through the k-means clustering methods (*kmeans* function, 'stats' R package). Points were mirrored on the left side and projected onto the surface to generate a bilateral set of semilandmarks. The final set of semilandmarks consists of 120 bilateral semilandmarks for endocasts and 200 for skulls. The final configurations of both landmarks and semilandmarks were symmetrized by using the function *symmetrize* embedded in the R package 'Morpho'[64]. Within the function *symmetrize*, the landmarks are reflected and relabeled according to the given indication of right and left indices. The original and the reflected configurations are then averaged to obtain a perfectly symmetric one.

To remove the size, orientation, and translation effect, we performed a Procrustes superimposition of the coordinates of both endocasts and skulls datasets. We computed the Principal Component Analysis (PCA) of partial warp scores (Relative Warp Analysis, RWA) to reduce data dimensionality and to explore the morphological endocasts and skulls shape variations. The Procrustes superimposition and the RWA were performed through the function *relWarps* in 'Morpho'.

Phylogenetic tree and RRphylo

We built two different informal supertrees including all Primate species related to the endocast and the skull dataset, using the function *tree.merger*[65] in the package 'RRphylo'. Our main reference for primate phylogenetic positions and last appearance ages is ref. 66. Last appearance ages for

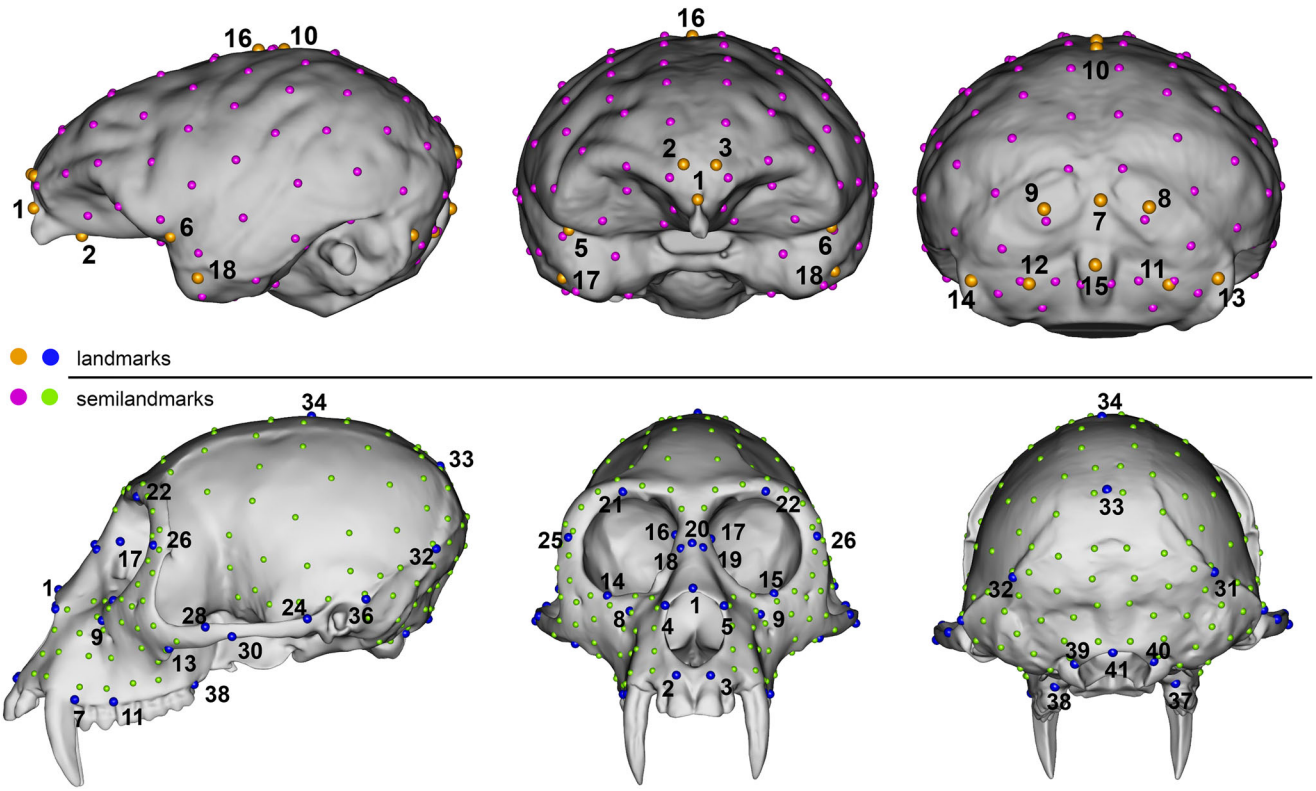

Fig. 5 | Endocast ($n = 18$) and cranium ($n = 41$) landmark configurations. Manually placed landmarks are numbered. The anatomical descriptions are reported in Supplementary Tables 1 and 2. Surface semilandmarks on endocast and cranium are respectively fuchsia and green.

missing species are indicated in Supplementary Data 2. The final tree for the endocast dataset includes 120 species (112 extant and 8 extinct), whereas for the skull dataset we included 93 species (88 extant, 5 extinct).

We estimated the rates of endocast evolution by applying the *RRphylo* method[26]. Rates were used to (1) map the areas of the Primate endocasts characterized by highest (and lowest) evolutionary rate values (*rate.map* case study); (2) compute possible instances of morphological convergence among Primate skulls with the function *search.conv*[67] in 'RRphylo' and visualize the strength of convergence on digital surfaces (*conv.map* case study on skulls); and (3) compare the pattern of convergence of endocast and skulls (*conv.map* case study).

RRmorph

'RRmorph' is a brand-new R package providing tools to map phenotypic evolutionary changes and patterns over 3D digital models in a phylogenetic framework. The main functions embedded in the package are meant to interpolate rate values, translated into changes in the triangles of a three-dimensional mesh in a given species or node in the tree as compared to the reference mesh's corresponding triangles. The main functions of 'RRmorph' are *conv.map* and *rate.map*. They were presented separately in two different papers by Melchionna et al.[28] and Castiglione et al.[27] and now updated to provide mapping on the original 3D mesh. In brief, *conv.map* charts patterns of convergence between pair-species on three-dimensional models by selecting the Principal Component (or Relative Warp) axes implied in convergence. After the PC selection, *conv.map* restores the shapes and surfaces of the paired species starting from the selected PCs or RWs, that is the portion of the morphological variance responsible for convergence. The triangle-by-triangle area differences between the restored surfaces and the consensus shape are computed. The resulting area differences are then compared between each other. Convergent areas will therefore present the smallest shape variation (plotted in color shades), whereas non-convergent regions will be plotted in white.

The *rate.map* algorithm is based on the same principle, but the selected PCs or RWs of compared species pairs are the ones associated with the highest (and lowest) evolutionary rates relatively to their common ancestors (for most applications the tree root).

In both *conv.map* and *rate.map* the surface reconstruction is automatically performed with the Ball-Pivoting algorithm[68] implemented in the *vcgBallPivoting* function ('Rcvg' R package[69]). The resulting triangular surfaces highly depend on the original pattern of landmarks and semilandmarks, and the area differences (species-species for convergence, or species to ancestor for the evolutionary rates) are associated to the mesh triangles. Here we implement both algorithms, to chart the convergence and the phenotypic change attached to the evolutionary rates on real surfaces. To this aim, we introduce an interpolation method which transfers the information associated to individual triangles of the reconstructed surfaces onto the corresponding triangles of the real digital models. The same interpolation can be performed if the value to be interpolated refers to the landmarks, rather than to the triangles. The interpolation is by a new algorithm named *interpoolMesh*, whose functioning is illustrated in Fig. 6. The first step of *interpoolMesh* is to compute the barycenter of each triangle of the reconstructed surfaces. Through the location of landmarks and semilandmarks on the real mesh, which corresponds to the vertices of the reconstructed surface, the position of the barycenter onto the real mesh is retrieved. After that, for each point of the real mesh (i.e. red dot in Fig. 6b) k barycenter (here to for nearest neighbor points, NNPs) are identified, and the Euclidean mean of the associated values is computed. The default value of k is equal to 4, as shown in Fig. 6. Subsequently, the real mesh is colored based on the interpolated values with the 'RRmorph' function *col2mesh*.

rate.map case study on endocasts

We computed evolutionary rates on the endocast Primate dataset with *RRphylo*. Then we ran *rate.map* by comparing each tip of the phylogenetic tree with the common ancestor (the root of the tree).

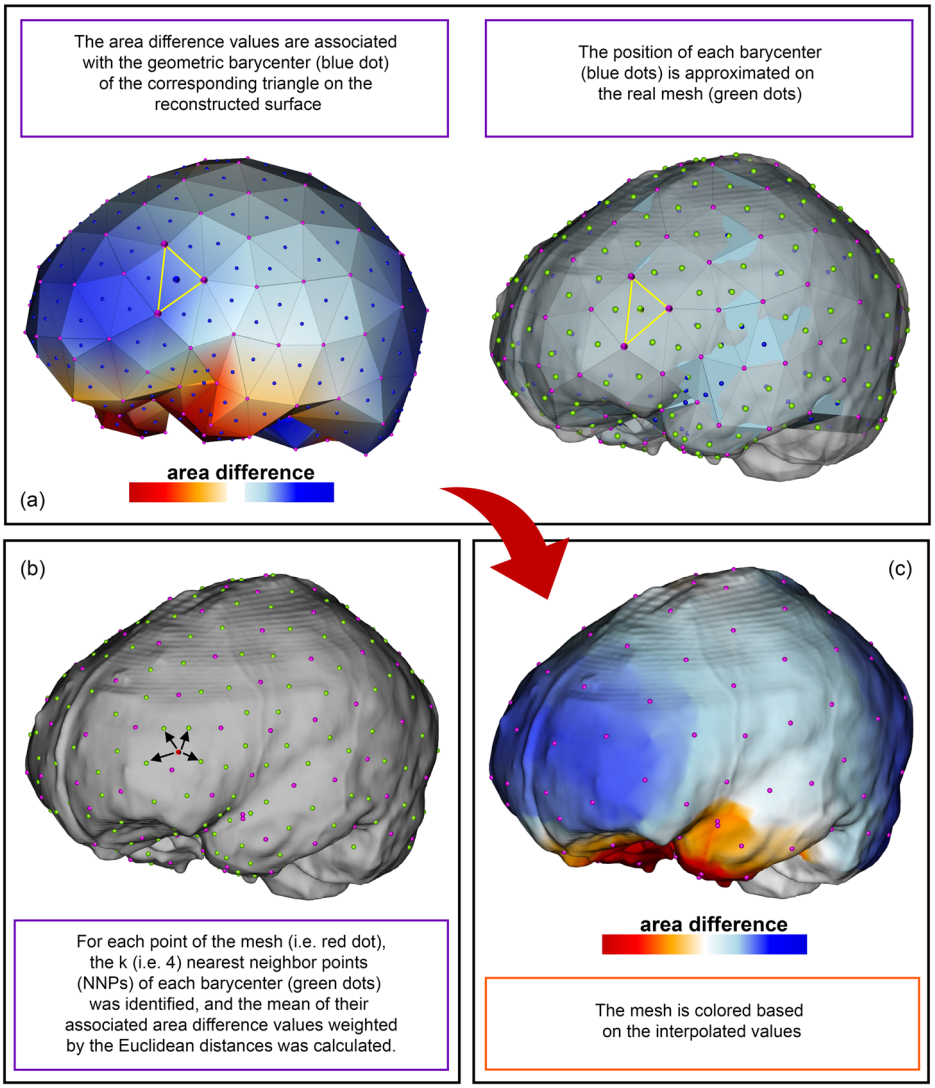

Fig. 6 | The interpolation machinery implemented in *rate.map* and *conv.map* embedded in 'RRmorph'. The steps (**a, b**) are performed by the 'RRmorph' function *interpoolMesh*. The step described in the orange box (**c**) is implemented by the 'RRmorph' function *col2mesh*.

conv.map case study on skulls

We computed evolutionary rates on the skulls dataset with *RRphylo*. We assessed the presence of the morphological convergence among Primate cranial shape with *search.conv*, an algorithm embedded in the R package 'RRphylo'[26], which tests whether unrelated clades are morphologically more similar to each other than expected by their phylogenetic distance. We used *conv.map* to compare species pairs that result to be convergent by mapping the convergence on three-dimensional surfaces.

conv.map case study on endocast and skulls

We decided to search for convergence by using a reduced dataset of both endocast and skulls, retrieved from the same individuals. Our aim is to see if the convergence regards the same clades and if a similar pattern of convergence is recognizable through *conv.map*.

Statistics and reproducibility

Statistical analysis was done with R Studio Software version 2023.06.0 based on R 4.4.0. A new package, 'RRmorph', was specifically created to perform the analyses presented here. RRmorph is mainly bases on the functions present in the R packages 'RRphylo'[26], 'Morpho' and 'Rcvg'[69]. Digital models of the skull were either downloaded from public repositories or provided by colleagues. The full list of specimen provenances is available as Supplementary Data 1. Specimens were processed to extract the endocasts via the R software *endomaker*[70] available within the R package 'Arothron'[71]. CT and laser scans were processed in Amira[63] and the resulting models landmarked with this same software. Rate analysis was performed with the function *RRphylo*[26]. Convergence was assessed using the theta statistics[67] which internally performs a randomization procedure to assess whether the angle between the PC score vectors (of any pair of species) weighted by their patristic distance is larger than expected by chance. The R codes to perform all of the analyses are available as online attachments to this manuscript. Figures and plots were prepared using the R package *ggplot2*[72] and the Photoshop suite.

Reporting summary

Further information on research design is available in the Nature Portfolio Reporting Summary linked to this article.

Data availability

The source information for the primate specimens included in the analyses is specified in the Supplementary Data 1. Age of extinction and source information for the phylogenetic positioning of species is reported in the Supplementary Data 2.

Code availability

The R scripts to perform the analyses along with datafiles to reproduce the examples presented in the manuscript are available via Dryad[73] repository at https://doi.org/10.5061/dryad.ksn02v7d0. The RRmorph[74] R package is available from Zenodo at https://doi.org/10.5281/zenodo.11658855.

Received: 24 April 2024; Accepted: 9 August 2024;
Published online: 17 August 2024

References

1. Freckleton, R. P. & Harvey, P. H. Detecting non-brownian trait evolution in adaptive radiations. *PLoS Biol.* **4**, 2104–2111 (2006).
2. Martins, E. P. Estimating the rate of phenotypic evolution from comparative data. *Am. Nat.* **144**, 193–209 (1994).
3. Gingerich, P. D. Rates of evolution. *Annu Rev. Ecol. Evol. Syst.* **40**, 657–675 (2009).
4. Harmon, L. J., Schulte, J. A., Larson, A. & Losos, J. B. Tempo and mode of evolutionary radiation in iguanian lizards. *Science (1979)* **301**, 961–964 (2003).
5. Cooney, C. R. et al. Mega-evolutionary dynamics of the adaptive radiation of birds. *Nature* **542**, 344–347 (2017).
6. Slater, G. J. Iterative adaptive radiations of fossil canids show no evidence for diversity-dependent trait evolution. *Proc. Natl Acad. Sci. USA* **112**, 4897–4902 (2015).
7. Hunt, G., Hopkins, M. J. & Lidgard, S. Simple versus complex models of trait evolution and stasis as a response to environmental change. *Proc. Natl Acad. Sci.* **112**, 4885–4890 (2015).
8. Beaulieu, J. M., Jhwueng, D. C., Boettiger, C. & O'Meara, B. C. Modeling stabilizing selection: expanding the Ornstein-Uhlenbeck model of adaptive evolution. *Evolution (N. Y)* **66**, 2369–2383 (2012).
9. Monroe, M. J. & Bokma, F. Does density-dependent diversification mirror ecological competitive exclusion? *PLoS One* **12**, e0184814 (2017).
10. Xu, L., Van Doorn, S., Hildenbrandt, H. & Etienne, R. S. Inferring the effect of species interactions on trait evolution. *Syst. Biol.* **70**, 463–479 (2021).
11. O'Meara, B. C. Evolutionary inferences from phylogenies: a review of methods. *Annu Rev. Ecol. Evol. Syst.* **43**, 267–285 (2012).
12. Zelditch, M. L., Li, J., Tran, L. A. P. & Swiderski, D. L. Relationships of diversity, disparity, and their evolutionary rates in squirrels (Sciuridae). *Evolution (N. Y)* **69**, 1284–1300 (2015).
13. Guillerme, T. dispRity: A modular R package for measuring disparity. *Methods Ecol. Evol.* **9**, 1755–1763 (2018).
14. Zimova, M. et al. Body size predicts the rate of contemporary morphological change in birds. *Proc. Natl Acad. Sci. USA* **120**, e2206971120 (2023).
15. Crawford, F. W. & Suchard, M. A. Diversity, disparity, and evolutionary rate estimation for unresolved Yule trees. *Syst. Biol.* **62**, 439–455 (2013).
16. Rabosky, D. L. Phylogenetic tests for evolutionary innovation: The problematic link between key innovations and exceptional diversification. *Philos. Trans. R Soc. B Biol. Sci.* **372**, 20160417 (2017).
17. Donoghue, M. J. Key innovations, convergence, and success: macroevolutionary lessons from plant phylogeny. *Paleobiology* **31**, 77–93 (2005).
18. Hunter, J. P. & Jernvall, J. The hypocone as a key innovation in mammalian evolution. *Proc. Natl Acad. Sci. USA* **92**, 10718–10722 (1995).
19. Emlen, D. J. The evolution of animal weapons. *Annu Rev. Ecol. Evol. Syst.* **39**, 387–413 (2008).
20. Raia, P., Carotenuto, F., Passaro, F., Fulgione, D. & Fortelius, M. Ecological specialization in fossil mammals explains Cope's rule. *Am. Nat.* **179**, 328–337 (2012).
21. Puttick, M. N., Thomas, G. H. & Benton, M. J. High rates of evolution preceded the origin of birds. *Evolution (NY)* **68**, 1497–1510 (2014).
22. Chatar, N., Fischer, V. & Tseng, Z. J. Many-to-one function of cat-like mandibles highlights a continuum of sabre-tooth adaptations. *Proc. R. Soc. B Biol. Sci.* **289**, 20221627 (2022).
23. Sansalone, G. et al. Decoupling Functional and Morphological Convergence, the Study Case of Fossorial Mammalia. *Front Earth Sci. (Lausanne)* **8**, 1–10 (2020).
24. Sansalone, G., Wroe, S., Coates, G., Attard, M. R. G. & Fruciano, C. Unexpectedly uneven distribution of functional trade-offs explains cranial morphological diversity in carnivores. *Nat. Commun. 2024 15:1* **15**, 1–15 (2024).
25. Janis, C. M. Who was the real sabertooth predator: Thylacosmilus or Thylacoleo? *Anat. Rec.* https://doi.org/10.1002/ar.25444 (2024).
26. Castiglione, S. et al. A new method for testing evolutionary rate variation and shifts in phenotypic evolution. *Methods Ecol. Evol.* **9**, 974–983 (2018).
27. Castiglione, S. et al. Human face-off: a new method for mapping evolutionary rates on three-dimensional digital models. *Palaeontology* **65**, 1–10 (2022).
28. Melchionna, M. et al. A method for mapping morphological convergence on three-dimensional digital models: the case of the mammalian sabre-tooth. *Palaeontology* **64**, 573–584 (2021).
29. Kratsch, C. & McHardy, A. C. RidgeRace: Ridge regression for continuous ancestral character estimation on phylogenetic trees. *Bioinformatics* **30**, 527–533 (2014).
30. Amiez, C. et al. Sulcal organization in the medial frontal cortex provides insights into primate brain evolution. *Nat. Commun.* **10**, 3437 (2019).
31. Hayashi, T. et al. Macaques exhibit implicit gaze bias anticipating others' false-belief-driven actions via medial prefrontal cortex. *Cell Rep.* **30**, 4433–4444.e5 (2020).
32. Smaers, J. B., Gómez-Robles, A., Parks, A. N. & Sherwood, C. C. Exceptional evolutionary expansion of prefrontal cortex in great apes and humans. *Curr. Biol.* **27**, 714–720 (2017).
33. Donahue, C. J., Glasser, M. F., Preuss, T. M., Rilling, J. K. & Van Essen, D. C. Quantitative assessment of prefrontal cortex in humans relative to nonhuman primates. *Proc. Natl Acad. Sci. USA* **115**, E5183–E5192 (2018).
34. Barton, R. A. & Venditti, C. Human frontal lobes are not relatively large. *Proc. Natl Acad. Sci. USA* **110**, 9001–9006 (2013).
35. Barton, R. A. & Montgomery, S. H. Proportional versus relative size as metrics in human brain evolution. *Proc. Natl Acad. Sci. USA* **116**, 3–4 (2019).
36. Schwartz, E. et al. Evolution of cortical geometry and its link to function, behaviour and ecology. *Nat. Commun.* **14**, 2252 (2023).
37. Ravosa, M. J. & Savakova, D. G. Euprimate origins: the eyes have it. *J. Hum. Evol.* **46**, 355–362 (2004).
38. Martin, R. D. & Ross, C. F. The evolutionary and ecological context of primate vision. In *The Primate Visual System* (ed. Kremers, J.) 1–36 (Wiley, 2005).
39. Hine, E., McGuigan, K. & Blows, M. W. Evolutionary constraints in high-dimensional trait sets. *Am. Nat.* **184**, 119–131 (2014).
40. Bennett, J. M. et al. The evolution of critical thermal limits of life on earth. *Nat. Commun.* **12**, 1198 (2021).
41. Fabre, A.-C. et al. Metamorphosis shapes cranial diversity and rate of evolution in salamanders. *Nat. Ecol. Evol.* **4**, 1129–1140 (2020).
42. Losos, J. B. Convergence, adaptation, and constraint. *Evolution (N. Y)* **65**, 1827–1840 (2011).
43. Sansalone, G. et al. Trapped in the morphospace: The relationship between morphological integration and functional performance. *Evolution* **76**, 2020–2031 (2022).
44. Meachen-Samuels, J. A. Morphological convergence of the prey-killing arsenal of sabertooth predators. *Paleobiology* **38**, 1–14 (2012).
45. Randau, M., Carbone, C. & Turvey, S. T. Canine evolution in sabretoothed carnivores: natural selection or sexual selection? *PLoS One* **8**, e72868 (2013).
46. Antón, M. et al. Implications of the mastoid anatomy of larger extant felids for the evolution and predatory behaviour of sabretoothed cats (Mammalia, Carnivora, Felidae). *Zool. J. Linn. Soc.* **140**, 207–221 (2004).
47. Sakamoto, M. & Venditti, C. Phylogenetic non-independence in rates of trait evolution. *Biol. Lett.* https://doi.org/10.1098/rsbl.2018.0502 (2018).
48. O'Meara, B. C., Ané, C., Sanderson, M. J. & Wainwright, P. C. Testing for different rates of continuous trait evolution using likelihood. *Evolution (N. Y)* **60**, 922 (2006).

49. Passingham, R. E. & Smaers, J. B. Is the prefrontal cortex especially enlarged in the human brain? allometric relations and remapping factors. *Brain Behav. Evol.* **84**, 156–166 (2014).
50. Gangopadhyay, P., Chawla, M., Dal Monte, O. & Chang, S. W. C. Prefrontal–amygdala circuits in social decision-making. *Nat. Neurosci.* **24**, 5–18 (2021).
51. Hiser, J. & Koenigs, M. The multifaceted role of the ventromedial prefrontal cortex in emotion, decision making, social cognition, and psychopathology. *Biol. Psychiatry* **83**, 638–647 (2018).
52. Turnbull, A. et al. Left dorsolateral prefrontal cortex supports context-dependent prioritisation of off-task thought. *Nat. Commun.* **10**, 3816 (2019).
53. Carlén, M. What constitutes the prefrontal cortex? *Science (1979)* **358**, 478–482 (2017).
54. Barton, R. A. & Venditti, C. Rapid evolution of the cerebellum in humans and other great apes. *Curr. Biol.* **24**, 2440–2444 (2014).
55. Smaers, J. B. & Vanier, D. R. Brain size expansion in primates and humans is explained by a selective modular expansion of the cortico-cerebellar system. *Cortex* **118**, 292–305 (2019).
56. Fiorenza, L. & Bruner, E. Cranial shape variation in adult howler monkeys (*Alouatta seniculus*). *Am. J. Primatol.* https://doi.org/10.1002/ajp.22729 (2018).
57. Bruner, E., Mantini, S. & Manzi, G. A geometric morphometric approach to airorhynchy and functional cranial morphology in Alouatta (Atelidae, Primates). *J. Anthropol. Sci.* **82**, 47–66 (2004).
58. Villamil, C. I. Locomotion and basicranial anatomy in primates and marsupials. *J. Hum. Evol.* **111**, 163–178 (2017).
59. Profico, A. et al. The evolution of cranial base and face in Cercopithecoidea and Hominoidea: modularity and morphological integration. *Am. J. Primatol.* **79**, 1–12 (2017).
60. Tattersall, I. The functional significance of airorhynchy in Megaladapis. *Folia Primatol.* **18**, 20–26 (2008).
61. Schwartz, G. T. et al. Dental development in Megaladapis edwardsi (Primates, Lemuriformes): implications for understanding life history variation in subfossil lemurs. *J. Hum. Evol.* **49**, 702–721 (2005).
62. Lautenschlager, S., Figueirido, B., Cashmore, D. D., Bendel, E. M. & Stubbs, T. L. Morphological convergence obscures functional diversity in sabre-toothed carnivores: sabre-tooth functional morphology. *Proc. R Soc B Biol. Sci.* https://doi.org/10.1098/rspb.2020.1818 (2020).
63. Stalling, D., Westerhoff, M. & Hege, H. C. Amira: A highly interactive system for visual data analysis. *Vis. Handb.* **1**, 749–767 (2005).
64. Schlager, S., Jefferis, G. & Dryden, I. *Morpho: Calculations and Visualisations Related to Geometric Morphometrics*. https://rdrr.io/cran/Morpho/ (2021).
65. Castiglione, S., Serio, C., Mondanaro, A., Melchionna, M. & Raia, P. Fast production of large, time-calibrated, informal supertrees with tree.merger. *Palaeontology* **65**, e12588 (2022).
66. Wisniewski, A. L., Lloyd, G. T. & Slater, G. J. Extant species fail to estimate ancestral geographical ranges at older nodes in primate phylogeny. *Proc. Royal Soc. B Biol. Sci.* **289**, 20212535 (2022).
67. Castiglione, S. et al. A new, fast method to search for morphological convergence with shape data. *PLoS One* **14**, e0226949 (2019).
68. Bernardini, F., Mittleman, J., Rushmeier, H., Silva, C. & Taubin, G. The ball-pivoting algorithm for surface reconstruction. *IEEE Trans. Vis. Comput. Graph* **5**, 349–359 (1999).
69. Schlager, S. In *Statistical Shape and Deformation Analysis: Methods, Implementation and Applications.* (eds. Zheng, G., Li, S., Szekely, G.) 508 (Academic Press Inc, 2017).
70. Profico, A., Buzi, C., Melchionna, M., Veneziano, A. & Raia, P. Endomaker, a new algorithm for fully automatic extraction of cranial endocasts and the calculation of their volumes. *Am. J. Phys. Anthropol.* **172**, 511–515 (2020).
71. Profico, A. et al. Arothron: An R package for geometric morphometric methods and virtual anthropology applications. *Am. J. Phys. Anthropol.* **176**, 144–151 (2021).
72. Wickham, H. et al. *ggplot2: Create Elegant Data Visualisations Using the Grammar of Graphics.* https://ggplot2.tidyverse.org (2023).
73. Melchionna, M. et al. RRmorph—Code and data to map phenotypic evolutionary rates and patterns on 3D meshes, for the case studies presented in this manuscript. https://doi.org/10.5061/dryad.ksn02v7d0 (2024).
74. Melchionna, M. et al. RRmorph R package. *Zenodo* https://doi.org/10.5281/zenodo.11658855 (2019).
75. Mérida, I. et al. CERMEP-IDB-MRXFDG: a database of 37 normal adult human brain [18F]FDG PET, T1 and FLAIR MRI, and CT images available for research. *EJNMMI Res.* **11**, 91 (2021).

Acknowledgements

The *Homo sapiens* brain MRI is part of copyrighted material "© Copyright CERMEP—Imagerie du vivant, www.cermep.fr and Hospices Civils de Lyon. All rights reserved". PR and MM are supported by grant 'Prin 2022 PNRR' emitted by the Ministry of University and Research (MUR).

Author contributions

M.M. and P.R. conceived the study. C.S., G.G., A.E. and M.M. performed landmark digitization and the statistical analyses. S.C. and M.M. prepared the RRmorph R package. A.P., G.S. and A.M. contributed in writing parts of the code. All authors contributed significantly to interpreting the data and results and writing the manuscript.

Competing interests

The authors declare no competing interests.

Additional information

Supplementary information The online version contains supplementary material available at https://doi.org/10.1038/s42003-024-06710-8.

Correspondence and requests for materials should be addressed to Marina Melchionna or Pasquale Raia.

Peer review information *Communications Biology* thanks Alessio Veneziano, and the other, anonymous, reviewers for their contribution to the peer review of this work. Primary Handling Editors: Aylin Bircan and Manuel Breuer. A peer review file is available.

Reprints and permissions information is available at http://www.nature.com/reprints

Publisher's note Springer Nature remains neutral with regard to jurisdictional claims in published maps and institutional affiliations.

Open Access This article is licensed under a Creative Commons Attribution-NonCommercial-NoDerivatives 4.0 International License, which permits any non-commercial use, sharing, distribution and reproduction in any medium or format, as long as you give appropriate credit to the original author(s) and the source, provide a link to the Creative Commons licence, and indicate if you modified the licensed material. You do not have permission under this licence to share adapted material derived from this article or parts of it. The images or other third party material in this article are included in the article's Creative Commons licence, unless indicated otherwise in a credit line to the material. If material is not included in the article's Creative Commons licence and your intended use is not permitted by statutory regulation or exceeds the permitted use, you will need to obtain permission directly from the copyright holder. To view a copy of this licence, visit http://creativecommons.org/licenses/by-nc-nd/4.0/.

© The Author(s) 2024